Computer Simulations of Static Stress-Strain States for Long-Length Pressurised Pipes with External Protective Thin Nanoengineered Coating under Nonuniform Temperature Fields

I.Sh. Nevliudov[1], A.G. Mamalis[2], Yu.V. Romashov[3]

[1]Kharkiv National University of Radio Electronics, Ukraine, Kharkiv, igor.nevliudov@nure.ua
[2]Project Center for Nanotechnology and Advanced Engineering, NCSR "Demokritos", Greece, Athens, a.mamalis@inn.demokritos.gr
[3]Kharkiv National University of Radio Electronics, Ukraine, Kharkiv
V.N. Karazin Kharkiv National University, Ukraine, Kharkiv, yurii.romashov@nure.ua

Influence of nonhomogeneous temperature fields on the stress-strain state of the pressurized pipes is due to temperature dependencies of the structural material properties like Young's module, Poisson's ratio and linear expansion coefficient, so that the nonuniform temperature fields leads to the inhomogeneous of the material properties. It is proposed to use the differential equations formulated through the displacement and the stresses to consider the stress-strain state for axisymmetric long-length pipes with external protective thin nanoengineered coating taking into account the nonuniform temperature fields. The finite differences are used to make the computer simulations of the pipes with the external protective thin nanoengineered coating, and the cladding of nuclear fuel rods made from the Zr-based alloy with the thin protective coating made from the stainless steel is considered as the example. It is shown that consideration of structural material properties temperature dependencies can have the noticeable influence on the stress-strain-state estimations for the pressurized pipes with external protective thin nanoengineered coating under nonuniform temperature fields.

Keywords: Pipes, thin coatings, stress-strain state, temperature field, computer simulation, nuclear fuel rod.

1. Introduction

The thin protective coatings are widely used for operability enhancing of different pressurised pipes including for the oil industry pipelines [1], for natural gas transportation pipelines [2], for steam boilers high-temperature pipes [3], for nuclear fuel claddings [4], as well as for other purposes. Effects of thin coating application is significant, so this idea has the further development, including through application of multilayers thin coatings [5], so that the researches about the pipes with thin protective coatings are in current interests at present, and a lot of existed scientific publications in this field confirm it.

The principal purpose of thin coating application for pressurized pipes is in corrosion protection of the main metal of the pipes from aggressive external mediums [6]. Different kinds of corrosion processes require developing of different protective coatings, so we have a lot of researches about the pipelines then coating to protect the particular kind of corrosion. The research [3] deals with the vanadium oxides induced high-temperature corrosion inherent for the steam boilers. The pipelines protective coatings to prevent the hydrogen embrittlement are considered in [7]. The specific corrosion processes of coated pipelines in soils taking into account of bacterial influencing are explored min [8]. At the same time, the protective coatings can be used to protect pipes not only from the corrosion, but also from other external influencing, including from the higher temperatures, like it is discussed in [9].

The implementation possibilities of thin coatings to protect the pipes are restricted by manufacturing capabilities and by the operability of such coatings under the pipes' exploitation conditions. In the research [10], the fabrication and behaviour investigation of new composite coating kinds for oils and gas pipelines are studied. The research [11] deals with studying about the manufacturing possibilities for making the internal coatings on the pipes. Possibilities of some manufacturing technology for making the nanocomposite coating with enhanced mechanical and corrosion protection are explored in [12]. Although, it is important to research influences of the manufacturing processes on the properties of pipes with thin protective coatings, but the principal difficulties are in anticipating these properties under the actual exploitation conditions of the pipes as the structural elements of complicated systems under influencing of different external factors. So, in the research [3], the corrosion processes from the vanadium oxide are considered taking into account a lot of different factors like the high temperature and the cyclic conditions. The crack safety of the cladding with the protective coating is considered in [13] with taking into account of the structural materials plastic behaviour. Protective thin coatings operability estimation is especially complicated for the claddings of nuclear fuel rods due to the specifics of the exploitation conditions in the cores of nuclear reactors, but this is principally required for design substantiation of the accident tolerant nuclear fuels [4]. The qualities of the coatings required to have the enhanced accident tolerant fuel claddings are researched in [14], and the performance of the nuclear reactor core loaded with such accident tolerance fuel is analysed in [15].

It is shown, that the mechanical properties [5] and effects like the plastic strains [13], elastic stresses [8,16] and others have significant influencing on the operability of the pressurized pipes with the thin protective coatings. In the previous researches [16, 17] it was shown that the thin protective coatings can lead to significant enhancing of the mechanical strength of the nuclear fuel rods claddings, so that it can be used to increase the general operability of the cladding. At the same time, it was shown [16], that the thermal strains have the

significant influence on the stress-strain state of the cladding, and it is really important for the claddings with the thin coatings due to the different values of heat expansion coefficients of the cladding's main material and the coating's materials. Nonuniform temperature fields lead to actually nonhomogeneous properties of structural material due to the temperature dependencies of the structural materials' mechanical properties. So, considering stress-strain states of the pipes with thin coatings under the nonuniform temperature fields requires using the computer simulations, because of the classical theoretical results [18] are built for the structures made from homogeneous materials. The purpose of this research is in developing of the approaches for making the computer simulations of static stress-strain states for long-length pressurised pipes with protective nanoengineering thin coatings taking into account the nonuniform temperature fields.

2. Mathematical model of the stress-strain state

We will consider the pressurized pipe as the cylinder with the internal radius and the external radius as well as with the length (fig. 1a). It will be assumed, that length of the pipe is significantly greater comparing with the external radius (fig. 1a):

$$L >> b. \tag{1}$$

In the case of axisymmetric loadings and temperature field, the stress-strain state of the pipe (fig. 1a) will be defined through the radial displacement, radial, circumferential and axial stresses depending only on the radial coordinate [18]:

$$u = u(r), \quad \sigma_r = \sigma_r(r), \quad \sigma_\theta = \sigma_\theta(r), \quad \sigma_z = \sigma_z(r), \quad a \le r \le b, \tag{2}$$

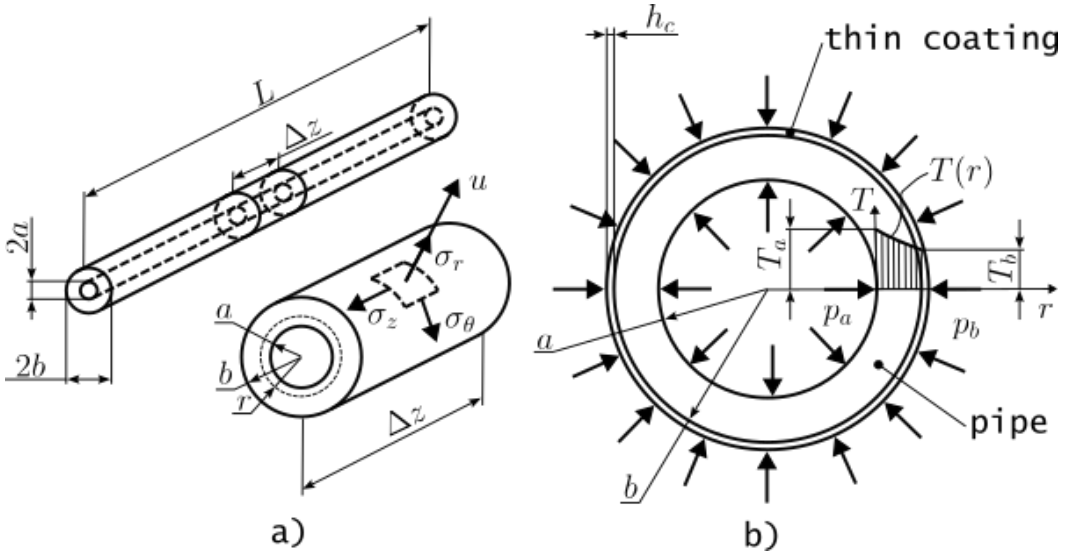

Figure 1 – The general schematisation (a) and the representative cross section (b) of the researched pipe with the external thin coating

where is the radial coordinate; is the radial displacement; is the radial stress; is the circumferential stress.

The displacement (2) leads to the following strains in the pipe [18]:

$$\varepsilon_r = \frac{du}{dr}, \quad \varepsilon_\theta = \frac{u}{r}, \quad \varepsilon_z = 0, \tag{3}$$

where ε_r, ε_θ and ε_z are the radial, circumferential and axial strains.

Due to the relations (1) and (3) we have the well-known plane strain problem of the theory of elasticity [18], so to represent the Hook's law for the researched elastic deformed pipe it is suitable to introduce the following values [16, 18]:

$$E = \frac{E'}{1-\nu'^2}, \ \nu = \frac{\nu'}{1-\nu'}, \ \alpha = (1+\nu')\alpha', \tag{4}$$

where E, ν and α are the equivalent Young's module, the Poisson's ratio and the linear expansion coefficient, but E', ν' and α' are the Young's module, the Poisson's ratio and the linear expansion coefficient of the material of the pipe.

We will consider further the elastic behaviour of the researched pipe (fig. 1a) taking into account the temperature field [16] (fig. 1b):

$$T(r) = \frac{T_a - T_b}{\ln a - \ln b}\ln r + \frac{T_b \ln a - T_a \ln b}{\ln a - \ln b}, \tag{5}$$

where T_a is the temperature on the internal radius of the pipe; T_b is the temperature on the external radius of the pipe.

The material properties are depended on the temperature:

$$E' = E'(T), \ \nu' = \nu'(T), \ \alpha' = \alpha'(T). \tag{6}$$

Due to the relations (4), (6), we will have nonhomogeneous structure material of the pipe in the case of nonuniform temperature field (5), so that:

$$E = E(T), \nu = \nu(T), \alpha = \alpha(T) \Rightarrow E = E(T(r)), \nu = \nu(T(r)), \alpha = \alpha(T(r)) \tag{7}$$

Taking into account the introduced values (4), the kinematic equations (3), the temperature field (5), the relations (7), the Hook's law for the elastic strains and the equilibrium equation [18], we will have the differential equations representing the stress-strain state of the researched pipe (fig. 1):

$$\frac{du}{dr} - \frac{1}{E}\sigma_r + \frac{\nu}{E}\sigma_\theta = \alpha\vartheta, \quad \frac{u}{r} + \frac{\nu}{E}\sigma_r - \frac{1}{E}\sigma_\theta = \alpha\vartheta, \quad a \le r \le b, \tag{8}$$

$$\frac{d\sigma_r}{dr}+\frac{\sigma_r-\sigma_\theta}{r}=0,\quad a<r<b, \tag{9}$$

where $\vartheta=\vartheta(r)$ is the relative temperature calculated from the temperature T_0 of naturally unloaded pipe, so that $\vartheta(r)=T(r)-T_0$.

To consider the pressurized pipe with the external protective thin coating (fig. 1b) we will use the boundary conditions developed in [16]:

$$\sigma_r(a)=-p_a,\ \sigma_r(b)+\frac{E_c h_c}{b^2}u(b)=-p_b+\frac{\alpha_c E_c h_c}{b}\vartheta(b), \tag{10}$$

where h_c is the thickness of the external protective thin nanoengineered coating (fig. 1b); E_c, α_c are the Young's module and the linear expansion coefficient of the coating's material.

To find the axial stress it is necessary to use the known relation [18]:

$$\sigma_z=\nu'(\sigma_r+\sigma_\theta)-E'\alpha'\vartheta. \tag{11}$$

Thus, in the view (4), (5), (6)–(11) we have the mathematical model of the stress-strain state of the elastic deformed pipe with external protective thin nanoengineered coating under nonuniform temperature fields (fig. 1).

3. Defining the stress-strain state of the cladding

Solving differential equations (8), (9) with the boundary conditions (10) is the complicated task due to taking into account of the temperature dependencies (6) leading to the nonhomogeneous material of the pipe, so that the numerical methods are suitable, and the finite differences will be used to do it. As it is envisaged in finite differences method, we will introduce the grid with the nodes:

$$r_k=a+(k-1)\Delta r,\ k=1,2,\ldots,n,\ \Delta r=\frac{b-a}{n-1}, \tag{12}$$

where r_k is the grid node's coordinate; n is the total count of grid nodes and Δr is the step of the grid.

Due to the grid (12), we can introduce also the nodal values of the unknowns (2):

$$u_k=u(r_k),\ \sigma_{r(k)}=\sigma_r(r_k),\ \sigma_{\theta(k)}=\sigma_\theta(r_k),\ k=1,2,\ldots,n. \tag{13}$$

Besides, we can introduce the nodal values of the relative temperature involved in (8), and the nodal values of the pipe's material properties:

$$\vartheta_k=\vartheta(r_k),\ E_k=E(T(r_k)),\ \nu_k=\nu(T(r_k)),\ \alpha_k=\alpha(T(r_k)),\ k=1,2,\ldots,n. \tag{14}$$

Taking into account the grid (12), the definitions (13), (14), as well as the well-known approximate formulas for the derivatives we can represent the differential equations (8), (9) with the boundary conditions (11) as follows:

$$\frac{-3u_1+4u_2-u_3}{2\Delta r}+\frac{\nu_1}{E_1}\sigma_{\theta(1)}=\alpha_1\vartheta_1-\frac{p_a}{E_1},\quad \frac{u_1}{a}-\frac{1}{E_1}\sigma_{\theta(1)}=\alpha_1\vartheta_1+\frac{\nu_1}{E_1}p_a, \tag{15}$$

$$\frac{u_{k+1}-u_{k-1}}{2\Delta r}-\frac{1}{E_k}\sigma_{r(k)}+\frac{\nu_k}{E_k}\sigma_{\theta(k)}=\alpha_k\vartheta_k,$$

$$\frac{u_k}{r_k}+\frac{\nu_k}{E_k}\sigma_{r(k)}-\frac{1}{E_k}\sigma_{\theta(k)}=\alpha_k\vartheta_k,\ k=2,3,\ldots,n-1, \tag{16}$$

$$\frac{u_{n-2}-4u_{n-1}}{2\Delta r}+\left(\frac{3}{2\Delta r}+\frac{E_c}{E_n}\frac{h_c}{b^2}\right)u_n+\frac{\nu_n}{E_n}\sigma_{\theta(n)}=\left(\alpha_n+\alpha_c\frac{E_c}{E_n}\frac{h_c}{b}\right)\vartheta_n-\frac{p_b}{E_n},$$

$$\left(\frac{1}{b}+\nu_n\frac{E_c}{E_n}\frac{h_c}{b^2}\right)u_n-\frac{1}{E_n}\sigma_{\theta(n)}=\left(\alpha_n-\alpha_c\nu_n\frac{E_c}{E_n}\frac{h_c}{b}\right)\vartheta_n+\frac{\nu_n}{E_n}p_b, \tag{17}$$

$$\frac{\sigma_{r(2)}}{r_2}+\frac{\sigma_{r(3)}}{2\Delta r}-\frac{\sigma_{\theta(2)}}{r_2}=-\frac{p_a}{2\Delta r}, \tag{18}$$

$$\frac{\sigma_{r(k)}-\sigma_{r(k-1)}}{2\Delta r}+\frac{\sigma_{r(k)}}{r_k}-\frac{\sigma_{\theta(k)}}{r_k}=0,\ k=3,4,\ldots n-2, \tag{19}$$

$$-\frac{E_c h_c}{2\Delta r b^2}u_n-\frac{\sigma_{r(n-2)}}{2\Delta r}+\frac{\sigma_{r(n-1)}}{r_{n-1}}-\frac{\sigma_{\theta(n-1)}}{r_{n-1}}=\frac{1}{2\Delta r}\left(p_b-\alpha_c E_c\frac{h_c}{b}\vartheta_n\right). \tag{20}$$

The relations (15) represent the differential equations (8) for the grid node $k=1$, but the relations (16) represent the differential equations (8) for the grid nodes $k=2,3,\ldots,n-1$, and the relations (17) represent the differential equations (8) for the grid node $k=n$. Likewise, the relation (18) represents the differential equation (9) for the grid node $k=2$, but the relations (19) represent the differential equation (9) for the grid nodes $k=3,4,\ldots,n-2$, and the relation (20) represents the differential equation (9) for the grid node $k=n-1$. In the view (15)–(20) we have the system of linear algebraic equations to find the nodal values (13), but the boundary values of the radial stress must be found separately from the boundary conditions (10). The axial stresses must be found through the relation (11). To represent this system of linear algebraic equation, it is suitable to introduce the vectors:

$$\{u\}=\begin{pmatrix}u_1 & u_2 & \ldots & u_n\end{pmatrix}^T,$$

$$\{\sigma_r\}=\begin{pmatrix}\sigma_{r(2)} & \sigma_{r(3)} & \ldots & \sigma_{r(n-2)}\end{pmatrix}^T,\ \{\sigma_\theta\}=\begin{pmatrix}\sigma_{\theta(1)} & \sigma_{\theta(2)} & \ldots & \sigma_{\theta(n)}\end{pmatrix}^T. \tag{21}$$

Due to the introduced vectors (21), the linear equations (15)–(17) and (18)–(20) can be represented in the vector-matrix form:

$$\left[A_u\right]\{u\}+\left[A_r\right]\{\sigma_r\}+\left[A_\theta\right]\{\sigma_\theta\}=\{p_A\},\ \left[B_u\right]\{u\}+\left[B_r\right]\{\sigma_r\}+\left[B_\theta\right]\{\sigma_\theta\}=\{p_B\},\quad(22)$$

where $\left[A_u\right]$, $\left[A_r\right]$, $\left[A_\theta\right]$ and $\left[B_u\right]$, $\left[B_r\right]$, $\left[B_\theta\right]$ are the given matrices, but $\{p_A\}$ and $\{p_B\}$ are the given vectors.

The matrices and the vectors in (22) can be defined directly from the relations (15)–(20), but they are cumbersome, and we will not represent they here. We note only that the matrix $\left[A_u\right]$ has the sizes $2n\times n$, the matrix $\left[A_r\right]$ has the sizes $2n\times(n-2)$, the matrix $\left[A_\theta\right]$ has the sizes $2n\times n$, the matrix $\left[B_u\right]$ has the sizes $(n-2)\times n$, the matrix $\left[B_r\right]$ has the sizes $(n-2)\times(n-2)$, the matrix $\left[B_\theta\right]$ has the sizes $(n-2)\times n$, but the vector $\{p_A\}$ has the size n and the vector $\{p_B\}$ has the sizes $n-2$. The relation (22) allows us to represent the correspondent system of linear algebraic equations as:

$$\begin{bmatrix}\left[A_u\right] & \left[A_r\right] & \left[A_\theta\right]\\ \left[B_u\right] & \left[B_r\right] & \left[B_\theta\right]\end{bmatrix}\begin{Bmatrix}\{u\}\\ \{\sigma_r\}\\ \{\sigma_\theta\}\end{Bmatrix}=\begin{Bmatrix}\{p_A\}\\ \{p_B\}\end{Bmatrix}.\quad(23)$$

Thus, estimating of the stress-strain state of the pressurized pipe with the external protective nanoengineered thin coating (fig. 1) is reduced to solving the system of linear algebraic equations.

4. Computer simulations and discussing of the results

As the example, we will consider the pressurised pipe representing the nuclear fuel rod cladding made from the Zr-based alloy with the design similar to the well-known VVER-1000 nuclear reactor, but with the thin protective coating made from the stainless steel. The input data for the computer simulations will be following [16]:

$$a=3{,}9\ \text{mm},\quad b=4{,}55\ \text{mm},\ E_c=177\ \text{GPa},\ \alpha_c=17{,}5\cdot10^{-6}\text{K}^{-1},\ h_c=10\ \mu m,\quad(24)$$

$$p_a=10\ \text{MPa},\quad p_b=16\ \text{MPa},\quad T_a=340\ ^\circ\text{C},\quad T_b=300\ ^\circ\text{C},\quad T_0=20\ ^\circ\text{C}.\quad(25)$$

It is difficult to find the data about the temperature dependencies (6) of the structural materials properties in general and for the Zr-based alloy in particular, so we had found the data about the temperature dependency only for the linear expansion coefficient of the Zr-based alloy [19]. In this case we will neglect the temperature dependencies for the Young's module and the Poisson's ratio, and we will use the following values [16]:

$$E'=77\ \text{GPa},\quad \nu'=0{,}36.\quad(26)$$

At the same time, we will consider the temperature dependency for the linear expansion coefficient (fig. 3) regarding with the data from [19]. We can see (fig. 3), that the temperature dependency of the linear expansion coefficient for the Zr-based alloy has the complicated form, and to take it into account we will use the cubic splines to interpolate the known values. At the same time, to represent the temperature dependency for the linear expansion coefficient in the programs we will use the linear interpolation through the known and additional data estimated from the known data by means the cubic splines (fig. 3), so

that absolute difference between the linear interpolation and the cubic spline is smaller than $\varepsilon = 0,01 \cdot 10^{-6} \mathrm{K}^{-1}$. Such approach was proposed and used for representing the functional dependencies in the computer programs (see Acknowledgments).

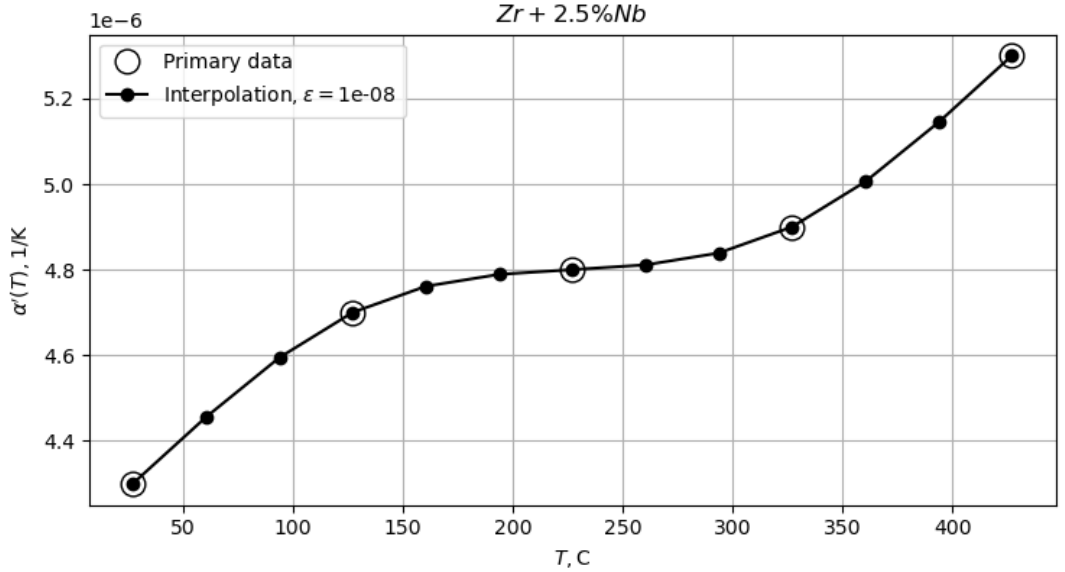

Figure 2 – Temperature dependency of the linear expansion coefficient

To make the computer simulations of the fuel rods cladding with the thin external protective coating (fig. 1), the Anaconda software with the Python programming language and Spider IDE are used to develop the scripts realising the proposed approach based on reduction of the problem to the system of linear algebraic equations (23). The well-known analytical solutions for the pressurized thick-walled cylinders [18] and the previous results [16] are used to substantiate the correctness of the developed scripts, so we can use these scripts for making the computer simulations further.

To illustrate the effect of material properties inhomogeneities due to the nonuniform temperature fields we will make the computer simulations taking into account the actual temperature dependence $\alpha' = \alpha'(T)$ of the linear expansion coefficient (fig. 2), as well as without considering this dependence for the given values of the linear expansion coefficients agreed with the temperatures (25) defining the temperature field in the researched cladding (fig. 1):

$$\alpha' = \alpha'(T_a) \cong 4,94 \cdot 10^{-6} \mathrm{K}^{-1}, \tag{27}$$

$$\alpha' = \alpha'(T_b) \cong 4,85 \cdot 10^{-6} \mathrm{K}^{-1}, \tag{28}$$

$$\alpha' = \alpha'\left(\frac{T_a + T_b}{2}\right) \cong 4,89 \cdot 10^{-6} \mathrm{K}^{-1}. \tag{29}$$

Although, the values (27)–(29) of the linear expansion coefficients are really close between each other, but some of the obtained results for the stress-strain state (fig. 3 – fig. 5) corresponded to these values have the noticeable differences.

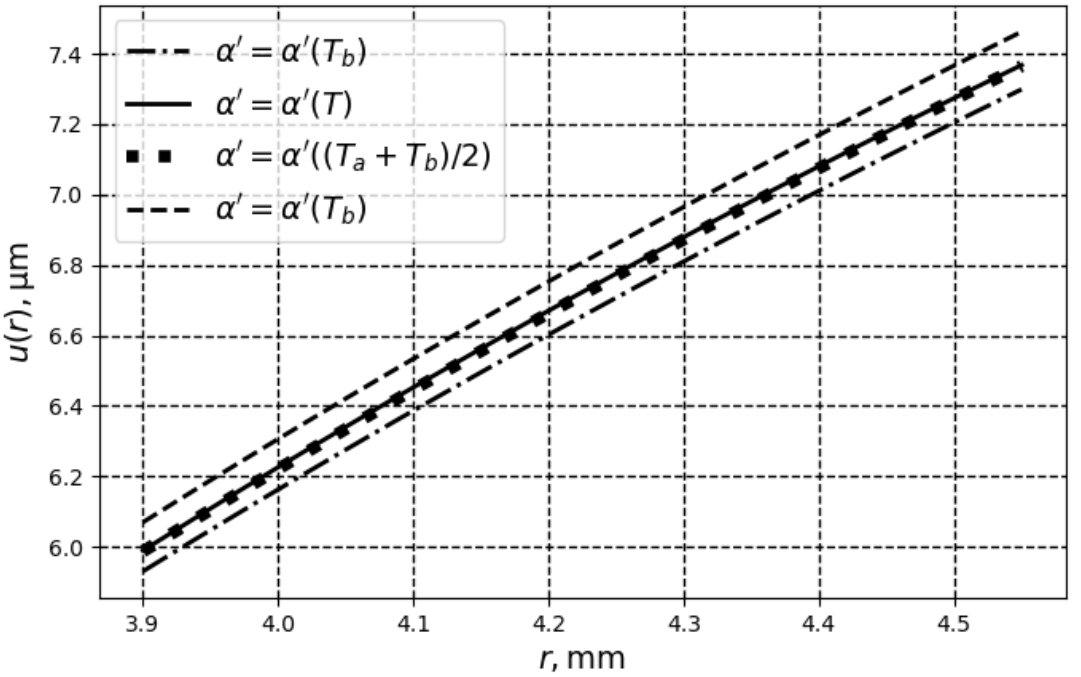

Figure 3 – The radial displacements estimations

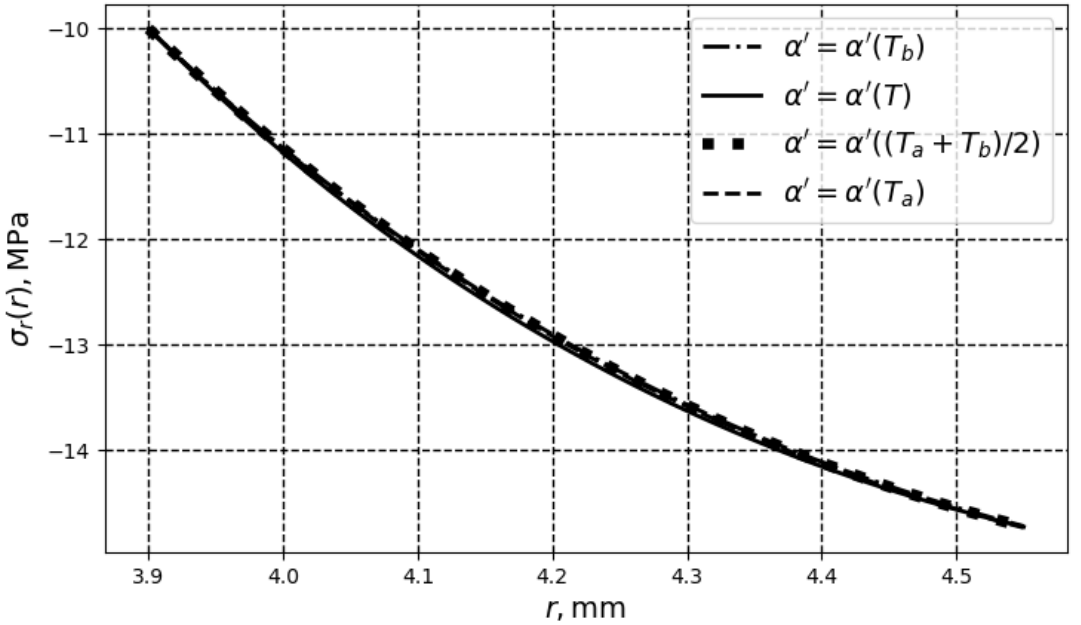

Figure 4 – The radial stress estimations

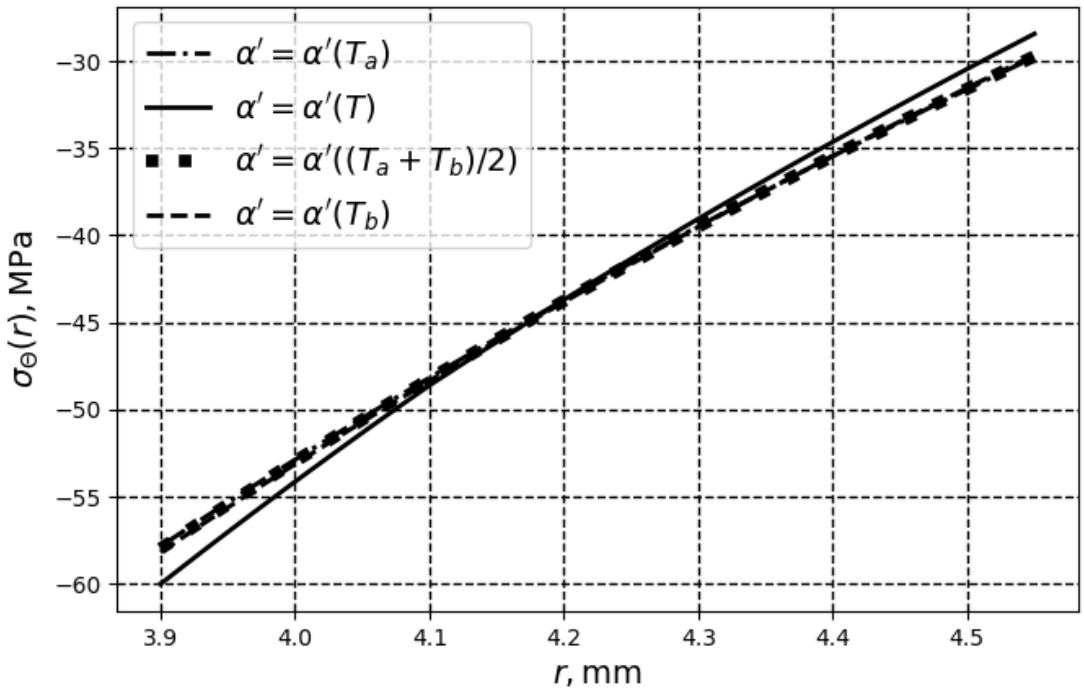

Figure 5 – The circumferential stress estimations

The results obtained for the radial displacements (fig. 3) and the radial stresses (fig. 4) shown that inhomogeneous of the linear expansion coefficient value induced by the nonuniform temperature field (5) have no noticeable influence. At the same time, we can see (fig. 4), that the inhomogeneous of the linear expansion coefficient value induced by the nonuniform temperature field (5) have the noticeable influence on the circumferential stresses. The different between the results on the fig. 4 is not principled for the static strength of the cladding, but it can be principled for damages accumulation processes in structural material, so it can lead to the different estimation for the long-term operability of the cladding. It is necessary to note, that the temperature dependencies of the Young's module and the Poisson's ration of the structural material are not considered in the results (fig.3 – fig. 5) obtained for the given constant values (26) of these characteristics, so the inhomogeneous of the material properties induced by the nonuniform temperature field (5) actually can be more significant.

Conclusions

Due to the accomplished researches presenting in this article, the following conclusion can be formulated.

It is suitable to use the differential equations formulated through the displacement and the stresses to make the computer simulations of the static stress-strain states of the axisymmetric long-length pipes with external protective thin nanoengineered coating taking into account the nonuniform temperature fields. These differential equations can be numerically solved by using the finite differences, and it can be realised through the Python programming language to have the primary results.

The inhomogeneous of the material properties induced by the nonuniform temperature fields have noticeable influence on circumferential stresses leading, but it has no effects on the radial stresses and radial displacements of the pipes with the external thin protective coating. These regularities are shown for the particular example, and it is impossible to distribute them to all the cases, so that to have the reliable estimation for the stress-strain states in the pipes with the thin coatings, it is necessary to make the computer simulations for each particular case.

To have the reliable estimations of the stress-strain states in the pressurized pipes with thin protective nanoengineered coatings under exploitational conditions leading to nonuniform temperature fields, it is necessary to take into account the actual temperature dependencies of the structural materials properties, but not the different constant values estimating these properties on the average or others different senses.

Acknowledgments

We would like to acknowledge to Daryna Nienova, student of the Computer Integrated Technologies, Automation and Mechatronics department of the Kharkiv National University of Radio Electronics for participation in development of the approaches providing the reliable functional dependencies representations, which was used to build fig. 2.

References

[1] Al Jabri, H., Devi, M.G., Al-Shukaili, M.A. Development of polyaniline – TiO2 nano composite films and its application in corrosion inhibition of oil pipelines. Journal of the Indian Chemical Society 100(1) (2023) 100826.

[2] Zhu, L., Tang, Y., Cao, S., Jiang, J., Wu, C., Zhao, K. Enhanced anti-microbial corrosion of nano-CuO-loaded Ni coatings on pipeline steels in simulation environment of natural gas transportation pipeline Ceramics International 49(3) (2023) 5543-5549.

[3] Singh, G., Bala, N., Chawla, V., Singla, Y.K. Hot corrosion behavior of HVOF-sprayed carbide based composite coatings for boiler steel in Na2SO4–60 % V2O5 environment at 900 °C under cyclic conditions. Corrosion Science 190 (2021) 109666.

[4] Yang, J., Steinbrück, M., Tang, C., Große, M., Liu, J., Zhang, J., Yun, D., Wang, S. Review on chromium coated zirconium alloy accident tolerant fuel cladding. Journal of Alloys and Compounds 895(1) (2022) 162450.

[5] He, H., Liu, C., He, L., Wang, G., Zhang, W., Zhao, S., Xiang, Y., Yi, J. Microstructure, mechanical properties and high temperature corrosion of [AlTiCrNiTa/(AlTiCrNiTa)N]20 high entropy alloy multilayer coatings for nuclear fuel cladding. Vacuum 212 (2023) 112057.

[6] Hussein Farh, H.M., Ben Seghier, M.E.A., Zayed, T. A comprehensive review of corrosion protection and control techniques for metallic pipelines. Engineering Failure Analysis 143(A) (2023) 106885.

[7] Lei, Y., Hosseini, E., Liu, L., Scholes, C.A., Kentish, S.E. Internal polymeric coating materials for preventing pipeline hydrogen embrittlement and a theoretical model of hydrogen diffusion through coated steel. International Journal of Hydrogen Energy 47(73) (2022) 31409-31419.

[8] Wei, B., Xu, J., Cheng, Y.F., Sun, C., Yu, C., Wang, Z. Effect of uniaxial elastic stress on corrosion of X80 pipeline steel in an acidic soil solution containing sulfate-reducing bacteria trapped under disbonded coating. Corrosion Science 193 (2021) 109893.

[9] Abu-warda, N., López, A.J., López, M.D., Utrilla, M.V. Ni20Cr coating on T24 steel pipes by

HVOF thermal spray for high temperature protection. Surface and Coatings Technology 381 (2020) 125133.

[10] MacLean, M., Farhat, Z., Jarjoura, G., Fayyad, E., Abdullah A., Hassan, M. Fabrication and investigation of the scratch and indentation behaviour of new generation Ni-P-nano-NiTi composite coating for oil and gas pipelines. Wear 426–427(A) (2019) 265-276.

[11] Sousa, F.A., da Costa, J.A.P., de Sousa, R.R.M., Barbosa, J.C.P., de Araújo, F.O. Internal coating of pipes using the cathodic cage plasma nitriding technique. Surfaces and Interfaces 21 (2020) 100691

[12] Sliem, M.H., Shahzad, K., Sivaprasad, V.N., Shakoor, R.A., Abdullah, A.M., Fayyaz, O., Kahraman, R., Umer, M.A. Enhanced mechanical and corrosion protection properties of pulse electrodeposited NiP-ZrO2 nanocomposite coatings. Surface and Coatings Technology 403 (2020) 126340.

[13] Wei, J., Xu, Z., Li, J., Liu, Y., Wang, B. Crack safety analysis of coating with plastic behavior in surface-coated Zircaloy cladding. Engineering Fracture Mechanics 280 (2023) 109134.

[14] Ridley, M., Bell, S., Garrison, B., Graening, T., Capps, N., Su, Y.-F., Mouche, P., Johnston, B., Kane, K. Effects of Cr/Zircaloy-4 coating qualities for enhanced accident tolerant fuel cladding. Annals of Nuclear Energy 188 (2023) 109799.

[15] Jeong, E., Jo, Y., Shin, C.H., Yang, Y.-S., Kim, J.-Y., Lee, D. Performance analysis of nuclear reactor core loaded with Accident-Tolerant Fuel: Mo/Cr metallic microcell UO2 pellets and CrAl coating. Annals of Nuclear Energy 175 (2022) 109217.

[16] Mamalis, A.G., Romashov, Yu.V. Enhanced operability of nuclear fuel rod cylindrical cladding made with thin protective nanoengineered coatings. Nanotechnology Perceptions 17(1) (2021) 74–81.

[17] Mazurenko, Yu.E., Romashov, Yu.V., Mamalis, A.G. Influencing of thin protective coatings on natural frequencies of radial oscillations of claddings of fuel rods of nuclear reactors. Voprosy Atomnoj Nauki i Tekhniki 1-125 (2020) 147–153.

[18] Timoshenko, S.P. and Goodier, J.N. Theory of Elasticity. New York: McGraw-Hill (1951).

[19] Thermophysical Properties of Materials for Nuclear Engineering: A Tutorial and Collection of Data. Vienna: International Atomic Energy Agency (2008).